



Liquid Crystals

Publication details, including instructions for authors and subscription information:

<http://www.tandfonline.com/loi/tlct20>

Wide-angle switchable negative refraction in high birefringence nematic liquid crystals

Dan Jia^{a b}, Chengliang Yang^a, Zenghui Peng^a, Xiaoping Li^{a b}, Yonggang Liu^a, Lishuang Yao^a, Zhaoliang Cao^a, Quanquan Mu^a, Lifa Hu^a, Xinghai Lu^a & Li Xuan^a

^a State Key Laboratory of Applied Optics, Changchun Institute of Optics, Fine Mechanics and Physics, Chinese Academy of Sciences, Jilin, 130033, China

^b Graduate School of the Chinese Academy of Sciences, Beijing, 100039, China

Published online: 26 Feb 2013.

To cite this article: Dan Jia, Chengliang Yang, Zenghui Peng, Xiaoping Li, Yonggang Liu, Lishuang Yao, Zhaoliang Cao, Quanquan Mu, Lifa Hu, Xinghai Lu & Li Xuan (2013) Wide-angle switchable negative refraction in high birefringence nematic liquid crystals, *Liquid Crystals*, 40:5, 599-604, DOI: [10.1080/02678292.2013.774065](https://doi.org/10.1080/02678292.2013.774065)

To link to this article: <http://dx.doi.org/10.1080/02678292.2013.774065>

PLEASE SCROLL DOWN FOR ARTICLE

Taylor & Francis makes every effort to ensure the accuracy of all the information (the "Content") contained in the publications on our platform. However, Taylor & Francis, our agents, and our licensors make no representations or warranties whatsoever as to the accuracy, completeness, or suitability for any purpose of the Content. Any opinions and views expressed in this publication are the opinions and views of the authors, and are not the views of or endorsed by Taylor & Francis. The accuracy of the Content should not be relied upon and should be independently verified with primary sources of information. Taylor and Francis shall not be liable for any losses, actions, claims, proceedings, demands, costs, expenses, damages, and other liabilities whatsoever or howsoever caused arising directly or indirectly in connection with, in relation to or arising out of the use of the Content.

This article may be used for research, teaching, and private study purposes. Any substantial or systematic reproduction, redistribution, reselling, loan, sub-licensing, systematic supply, or distribution in any form to anyone is expressly forbidden. Terms & Conditions of access and use can be found at <http://www.tandfonline.com/page/terms-and-conditions>

Wide-angle switchable negative refraction in high birefringence nematic liquid crystals

Dan Jia^{a,b}, Chengliang Yang^a, Zenghui Peng^a, Xiaoping Li^{a,b}, Yonggang Liu^a, Lishuang Yao^a, Zhaoliang Cao^a, Quanquan Mu^a, Lifa Hu^a, Xinghai Lu^a and Li Xuan^{a*}

^aState Key Laboratory of Applied Optics, Changchun Institute of Optics, Fine Mechanics and Physics, Chinese Academy of Sciences, Jilin 130033, China; ^bGraduate School of the Chinese Academy of Sciences, Beijing 100039, China

(Received 25 December 2012; final version received 4 February 2013)

Negative refraction (NR) is a promising technique that provides an opportunity to manipulate beam behaviour. We have demonstrated experimentally the controllable NR with large refraction angle at visible wavelength in the novel high birefringence (Δn) liquid crystals. When the Δn of liquid crystal reaches 0.42, the NR angle and critical incident angle reach -14° and 23.2° , respectively, which are much larger than those achieved before by other liquid crystals. By applying the electric field, we control the switch from NR to positive.

Keywords: negative refraction; nematic liquid crystal; high birefringence; low viscosity

1. Introduction

As a novel phenomenon, negative refraction (NR) was proposed conceptually by Veselago in 1968.[1] The metamaterials producing NR have been focused on extensively in superlens, optical cloaking and so on.[2–6] Many kinds of NR materials consisted of artificial structures have been studied in the past decade, such as the combination of metallic wire arrays and split resonant rings at microwave range [7–11] and metal-dielectric-metal structures at near-infrared wavelength range.[12–16] However, artificial structured materials have some disadvantages such as complex fabrication process and strong energy dissipation. As a result, many researchers devote to achieve NR in natural materials.[17–24] Zhang yong et al. studied NR in YO_4 crystals employing uniaxial property.[17–19] Pishnyak et al. [20] and Zhao et al. [21,22] observed NR in nematic liquid crystals (NLCs) which could be used for a variety of tunable optical devices [25–27] like beam steering and light router. According to the experiments reported in references [20–22], the maximum negative refraction angle (MNRA) is -7.7° and switch speed is up to tens of seconds,[20] which are too small and too slow for the applications. Also liquid crystals (LCs) have been widely employed to realise tunable NR [28–32] and the switch speed highly depends on the viscosity of LCs. Larger NR angle and faster switch speed are urgently required for practical use in NR area.

Here we focus on the NR phenomenon in NLCs. The critical parameters to describe the tunable NR ability of the NLC are the MNRA and the switch time. In this paper, three novel LC materials with

much higher birefringence (Δn) proposed in references [33–35] have been synthesised successfully by our group to enlarge the refractive angle. The LCs reported in reference [33] play an important part in shortening the switch time due to its lower viscosity. To the best of our knowledge, it is the first time that the tunable NR with so big MNRA is achieved by NLC experimentally.

2. Theory

The theory for NR in NLC has been introduced in references [20,21], so we only show the formulas instead of getting into details. The NLC cell lies in the X-Z plane and the interface ($Z = 0$) separates the air from the NLC as shown in Figure 1(a). The incident light is polarised in the plane of the figure. The direction of the molecular (director \mathbf{n}) is parallel to the cell substrates and inclined with an angle α to the Z axis. The incident angle is θ_i and the refractive angle is θ_r . If the refractive beam and the incident beam lay on the same side of the normal, NR is achieved.

The dispersion equation of the light can be obtained by solving the Maxwell's equations. In the air, the dispersion equation for the normalised components of the wave vector for transverse magnetic (TM) wave is

$$k_{ix}^2 + k_{iz}^2 = 1. \quad (1)$$

Where k_{ix} and k_{iz} are the x and z components of the wave vector k_i . In the NLC, the dispersion equation

*Corresponding author. Email: xuanli@ciomp.ac.cn

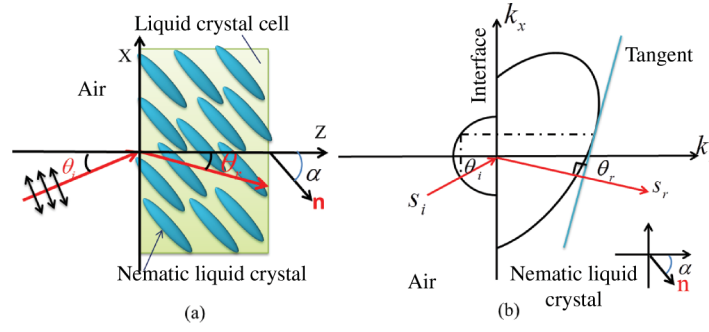


Figure 1. (colour online) (a) The sketch map of the NR in the NLC cell. (b) The wave vector surfaces in air and NLC.

of the normalised wave vector components for the extraordinary light (*e* light) is

$$\frac{(k_{rx} \cos \alpha + k_{rz} \sin \alpha)^2}{n_e^2} + \frac{(k_{rx} \sin \alpha - k_{rz} \cos \alpha)^2}{n_o^2} = 1. \quad (2)$$

Where k_{rx} and k_{rz} are the *x* and *z* components of the wave vector in the NLC, n_o and n_e are the refractive indices of the ordinary and extraordinary light. The wave vector surfaces can be obtained through Equations (1) and (2) which are shown in Figure 1(b). Because the tangential component of the wave vector is continuous on the boundary between the air and the NLC, one can find $k_{rx} = k_{ix}$. Substituting $k_{rx} = k_{ix}$ into Equation (2), the wave vector \mathbf{k}_r can be obtained. Using the Snell mapping method, the energy flow \mathbf{S}_r can be acquired as shown in Figure 1(b). The corresponding refractive angle is as follows:

$$\theta_r = \tan^{-1} \frac{2n_i \sin \theta_i + \sin 2\alpha(n_e^{-2} - n_o^{-2})n_o n_e \sqrt{(n_o^{-2} \cos^2 \alpha + n_e^{-2} \sin^2 \alpha)n_o^2 n_e^2 - n_i^2 \sin^2 \theta_i}}{2(n_o^{-2} \cos^2 \alpha + n_e^{-2} \sin^2 \alpha)n_o n_e \sqrt{(n_o^{-2} \cos^2 \alpha + n_e^{-2} \sin^2 \alpha)n_o^2 n_e^2 - n_i^2 \sin^2 \theta_i}}. \quad (3)$$

For a given α , the NR angle θ_r decreases when the incident angle θ_i increases. When $\theta_i = 0$ and $\alpha = \tan^{-1}(n_e/n_o)$ the MNRA can be achieved as

$$\theta_{\max} = -\tan^{-1}[(n_e^2 - n_o^2)/2n_o n_e]. \quad (4)$$

When the refractive angle $\theta_r = 0$, the corresponding incident angle θ_i is defined as the critical incident angle (CIA) which is given by

$$\theta_{\text{CIA}} = \arcsin \frac{\sin 2\alpha(n_e^2 - n_o^2) \sqrt{n_o^{-2} \cos^2 \alpha + n_e^{-2} \sin^2 \alpha}}{\sqrt{4 + \sin^2 2\alpha(n_e^{-2} - n_o^{-2})^2 n_o^2 n_e^2}}. \quad (5)$$

NR in NLCs originates from the optical Δn and occurs when the polarisation state of incident light is *p*

polarised and the incident angle is between zero and CIA. NLCs are not full-angle NR materials, so the MNRA and the CIA are the most important parameters for NR in NLC. From Equations (4) and (5), we can see that the MNRA and CIA are functions of n_o and n_e . Because n_o of LC material is almost a constant around 1.5, whether big MNRA and CIA can be achieved or not mainly depend on n_e . Therefore, the higher Δn results in the bigger MNRA and CIA.

3. Experimental details

3.1 The properties of the LC materials

Table 1 shows the properties of the LC materials investigated in this experiment. The Δn of LC1 (SLC9023, $n_o = 1.52$ and $n_e = 1.78$) is 0.26 at $\lambda = 532$ nm. LC2 was synthesised according to reference [33] (Δn is 0.39, $\lambda = 532$ nm). The isothio-

cyanate group (NCS group) in LC2 provides relatively long π -electron conjugation which is the reason for big Δn . The isothiocyanato-benzene in LC2 molecular reduces the intermolecular interaction, so its rotational viscosity is relatively low. LC3 [34,35] ($\Delta n = 0.5$, $\lambda = 532$ nm) and LC4 [34,35] ($\Delta n = 0.7$, $\lambda = 532$ nm) were also synthesised, but they are unable to be used directly in this experiment because they are solid at room temperature. Due to the compatibility between the LC materials, LC1 and LC2 are used as host to dissolve LC3 and LC4 in order to increase the Δn further.

Some properties of the new LC mixtures which are named as S1, S2, S3, S4 and S5 are showed in Table 2. According to the reference [34], the Δn value of the mixtures can be calculated as $\Delta n = \gamma(\Delta n)_1 + (1 - \gamma)(\Delta n)_2$, where the subscripts 1 and 2 denote different LC and γ is the mass fraction (in wt.%) of

Table 1. Properties of the liquid crystal materials in this experiment.

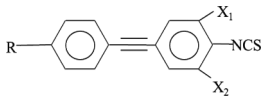
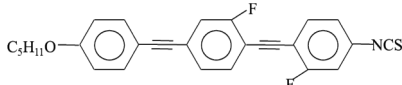
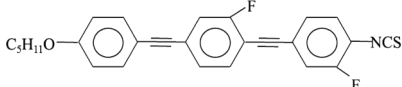
Liquid crystal	Molecular formula	$\Delta n, \lambda = 532 \text{ nm}$	State at room temperature
LC1	SLC9023	0.26	Liquid
LC2		0.39	Liquid
LC3		0.50	Solid
LC4		0.70	Solid

Table 2. Properties of mixtures.

Mixtures	Component(s)	$\Delta n, \lambda = 532 \text{ nm}$
S1	LC1	0.26
S2	16.7% LC3, 83.3% LC1	0.3
S3	18.2% LC4, 81.8% LC1	0.34
S4	LC2	0.39
S5	27.3% LC3, 72.7% LC2	0.42

the material with subscript 1. Finally, five new mixtures (S1–S5) whose Δn are 0.26, 0.3, 0.34, 0.39 and 0.42 respectively are obtained.

3.2 Preparation of LC cell

To demonstrate NR in NLC at visible wavelength, we designed and fabricated five LC cells. Each LC cell consists of two parallel glass substrates. Inside of each glass substrate, the transparent conductive film (ITO) is coated to drive the electric field. On each ITO film, polyimide (PI) film is coated and rubbed to arrange the LC molecular along its rubbing direction. The rubbing direction (\mathbf{n} as shown in Figure 1) is optimised through calculation. The optimal rubbing direction (angle α) between the rubbing direction and the Z axis is only decided by the refractive indices of the LC materials filled in the cell. The thickness of these LC cells is about 40 μm . The five LC mixtures (S1–S5) are filled in these cells (C1–C5) which are used in optical experiment in next section.

3.3 Experimental setup

The sketch map of the experimental setup is shown in Figure 2. The light source is a 532 nm solid state laser.

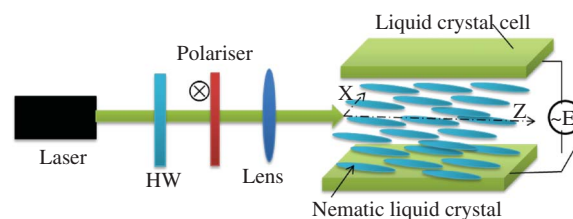


Figure 2. (colour online) The experimental setups for negative refraction in liquid crystal.

The polariser p and the half-waveplate (HW) are used to control the light intensity and polarisation. When the light goes through the polariser p , it becomes a linearly polarised light, whose polarisation direction is in the X-Z plane. Then the polarised light is focused by a long focal distance lens ($f = 200 \text{ mm}$) and the focal point is on the interface ($Z = 0$) of the LC cell. The diameter of the beam on the incident interface is about 20 μm , which is smaller than the thickness of the LC cell. These configurations make sure that the light can be coupled into the LC cell effectively and can propagate a long distance before diverging into the substrates. The LC cell is mounted on a sample stage with goniometer, so the incident angle can be controlled continuously. The propagation route of the beam in the NLC slab can be observed by human eye and recorded by a CCD camera.

4. Results and discussions

4.1 Negative refraction in NLC with high Δn

A NLC cell, marked C1, filled with S1 (SLC9023) is carefully mounted on the sample stage. The rubbing

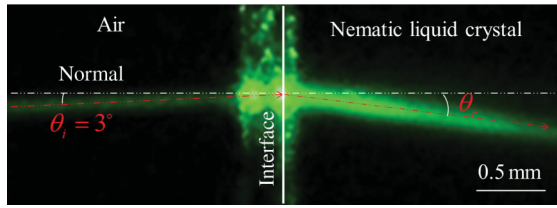


Figure 3. (colour online) The photograph of the negative refraction phenomena in NLC.

direction (angle α) of C1 is 40° which can be calculated from Equation (4). When the incident laser beam passes through the LC slab with 3° incident angle, the refractive angle is about -7.2° and the incident and refractive rays lay on the same side of the normal as shown in Figure 3. The refractive angle is negative when $0 \leq \theta_i \leq 14.7^\circ$. When the incident angle equals to zero, the MNRA (-9°) is accomplished.

Big MNRA is very important for the practical applications. Here we devote to obtain wide-angle NR in LC. As discussed in Section 2, the MNRA depends on the Δn of LC. When the Δn increases, the MNRA increases accordingly. In the experiment, four kinds of LC materials (S2–S5) with much higher Δn than the common commercial LCs were used to achieve the NR with much larger MNRA than reported before. Each of these LCs (S2–S5) mentioned earlier is filled into a LC cell to form a sample with its own rubbing direction α . In our experiment a group of the refractive angles for each sample are recorded for different incident angles with a step of 3° . The experimental data are shown in Figure 4. The corresponding theory prediction calculated by Equation (3) for each sample is also shown. Taking S5 as an example, the NR will appear in the incident angle range from 0° to 23.2° and the MNRA can get up to -14° . The experimental results agree well with the theory predictions. When the NR occurs, the value of the refractive angle goes smaller with the increasing incident angle. When

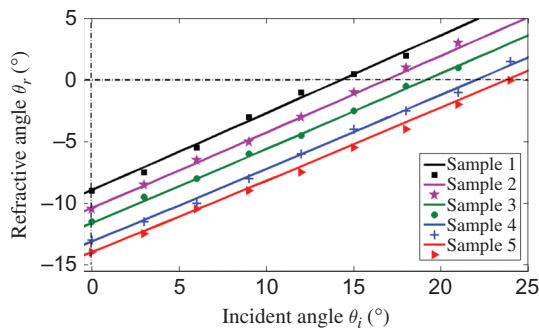


Figure 4. (colour online) The refractive angles for different incident angles. Discrete dots are experimental data and lines are theory calculations.

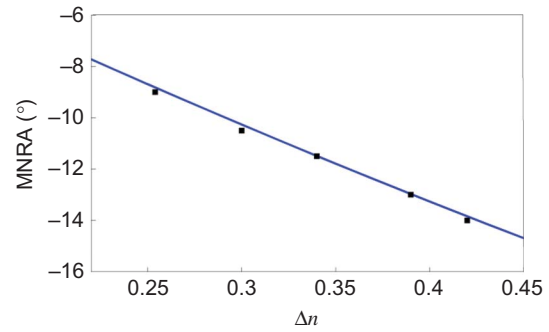


Figure 5. (colour online) The relation between the maximum negative refraction angle and Δn of LC.

the incident angle is close to zero, the corresponding refractive angle gets close to the MNRA. Meanwhile the CIA is measured when the refractive angle of each sample is equal to zero.

The relation between the MNRA and Δn for these five samples is shown in Figure 5. The square points are experimental data and the line is the theory prediction. From Figure 5 we can see that the magnitude of the MNRA increases with Δn and the experimental data are in good agreement with the theoretical prediction. When the Δn equals to 0.42, the MNRA reaches -14° that is almost one time larger than the value -7.7° reported before.[20] The magnitude of the CIA also increases with the Δn of LC. From Figure 4 the CIA increases from 14.7° to 23.2° when Δn increases from 0.26 (S1) to 0.42 (S5), which extensively expands the range of NR in LCs. Wide-range NR needs big Δn , as a result high molecular polarisation is required. The molecular polarisation can be further improved through molecular structure designs and chemosynthesis.

4.2 Switchable NR

As shown in Figure 6(a), the long axis of the LC molecular is parallel to the substrates of the LC cell. When the incident light is polarised in the plane of cell walls (X-Z plane, p polarised) and the incident angle is smaller than the CIA, the NR of the e light would occur in the LC slab as discussed earlier. If an electric field perpendicular to the LC slab is employed by applying a voltage on the ITO layer, the alignment of the LC molecular is changed to the direction of the electric field as shown in Figure 6(b). The e light in the LC slab changes to o light and the NR is switched to positive refraction (PR). As a result, the switch between NR and PR can be realised by controlling the electric field.

The switch time is closely related to the cell thickness and the rotational viscosity of the material.

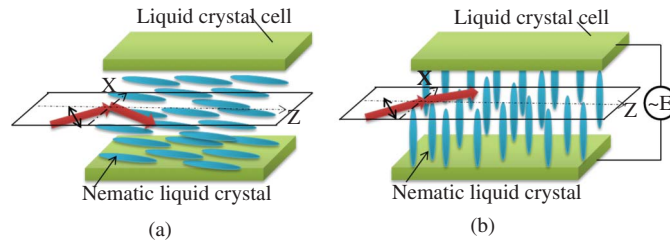


Figure 6. (colour online) The switch between negative refraction and positive refraction. (a) Without electric field, the NR occurs. (b) With electric field, the positive refraction occurs.

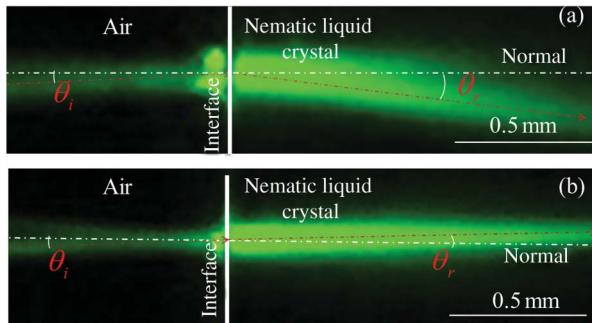


Figure 7. (colour online) Voltage-controlled switch experiments of negative refraction and positive refraction. (a) Without voltage (b) With voltage.

In order to let the beam propagate a longer distance in the NLC cell before diverging into the substrates, the long depth of focus is achieved by a long focal distance lens. The laser diameter on the interface is about $20\ \mu\text{m}$, so we adjust the cell thickness to be about $40\ \mu\text{m}$. So we cannot improve the response time by reducing the cell thickness, as a result the viscosity of the material plays a more important part in improving the response property of LCs.

The results of voltage-controlled switch experiments are shown in Figure 7. Without a voltage the NR occurred are shown in Figure 7(a). When a voltage is applied, the refraction becomes positive as shown in Figure 7(b). The switch time in the $40\ \mu\text{m}$ LC cell is about 50 seconds for S1–S3 and about 4 seconds for S4 and S5 which is one order faster than reported before.[20] Several methods can be used to improve the switch time, such as reducing the thickness of the LC cell. Employing the dual-frequency LC materials [36,37] is also a way to improve the response time and the work for designing and synthesising highly birefringent dual-frequency LC materials is ongoing now and the fast switchable wide-angle NR will be accomplished in these materials.

5. Conclusions

In summary, we have demonstrated large angle switchable NR experimentally through the high Δn

NLCs. By employing the new LC components, large NR angle is achieved in wide incident angle range. The critical angle reaches 23.2° and the MNRA reaches -14° which is one time larger than that achieved before in LC. Due to the switchable ability of the LC molecular under electric field, second order switch between NR and PR has been realised in $40\ \mu\text{m}$ LC cells through low viscosity LCs which is one order faster than NR in LCs reported before. Even faster response speed can be achieved by reducing the cell thickness or employing DFLC. The large NR angle and switchable properties make it a promising candidate for practical applications in optics.

Acknowledgements

This work was supported by the National Science Foundation of China (11174274, 11174279, 61205021 and 11204299) and the Science Foundation of State Key Laboratory of Applied Optics.

References

- [1] Veselago VG. The electrodynamics of substances with simultaneously negative values of ϵ and μ . *Sov Phys Usp.* 1968;10:509–514.
- [2] Pendry JB. Negative refraction makes a perfect lens. *Phys Rev Lett.* 2000;85:3966–3969.
- [3] Ziolkowski RW. Design, fabrication, and testing of double negative metamaterials. *IEEE Trans Antenn Propag.* 2003;51:1516–1529.
- [4] Cai W, Chettiar UK, Kildishev AV, Shalaev VM. Optical cloaking with metamaterials. *Nat Photonics.* 2007;1:224–227.
- [5] Zhang X, Liu Z. Superlenses to overcome the diffraction limit. *Nat Mater.* 2008;7:436–441.
- [6] Veselago VG, Narimanov EE. The left hand of brightness: past, present and future of negative index materials. *Nat Mater.* 2006;5:759–762.
- [7] Pendry JB, Holden AJ, Stewart WJ, Youngs I. Extremely low frequency plasmons in metallic mesostructures. *Phys Rev Lett.* 1996;76:4773–4776.
- [8] Pendry JB, Holden AJ, Robbins DJ, Stewart WJ. Magnetism from conductors and enhanced nonlinear phenomena. *IEEE Trans Microw Theory Tech.* 1999;47:2075–2084.

- [9] Smith DR, Padilla Willie J, Nemat-Nasser Vier DC, Schultz S. Composite medium with simultaneously negative permeability and permittivity. *Phys Rev Lett*. 2000;84:4184–4187.
- [10] Shelby RA, Smith DR, Schultz S. Experimental verification of a negative index of refraction. *Science*. 2001;292:77–79.
- [11] Shalaev VM. Optical negative-index metamaterials. *Nat Photonics*. 2007;1:41–48.
- [12] Shalaev VM, Cai W, Chettiar UK, Yuan HK, Sarychev AK, Drachev VP, Kildishev AV. Negative index of refraction in optical metamaterials. *Opt Lett*. 2005;30:3356–3358.
- [13] Dolling G, Enkrich C, Wegener M, Soukoulis CM, Linden S. Simultaneous negative phase and group velocity of light in a metamaterial. *Science*. 2006;312:892–894.
- [14] Hoffman AJ, Alekseyev L, Howard SS, Franz KJ, Wasserman D, Podolskiy VA, Narimanov EE, Sivo DL, Gmachl C. Negative refraction in semiconductor metamaterials. *Nat Mater*. 2007;6:946–950.
- [15] Mary A, Rodrigo SG, Garcia-Vidal FJ, Martin-Moreno L. Theory of negative-refractive-index response of double-fishnet structures. *Phys Rev Lett*. 2008;101:103902-1–103902-4.
- [16] Minovich A, Neshev DN, Powell DA, Shadrivov IV, Kivshar YS. Tunable fishnet metamaterials infiltrated by liquid crystals. *Appl Phys Lett*. 2010;96:193103-1–193103-3.
- [17] Yong Zhang B, Mascarenhas FA. Total negative refraction in real crystals for ballistic electrons and light. *Phys Rev Lett*. 2003;91:157404-1–157404-4.
- [18] Chen XL, He M, Du YX, Wang WY, Zhang DF. Negative refraction: an intrinsic property of uniaxial crystals. *Phys Rev B*. 2005;72:113111-1–113111-4.
- [19] Du YX, He M, Chen XL, Wang WY, Zhang DF. Uniaxial crystal slabs as amphoteric-reflecting media. *Phys Rev B*. 2006;73:245110-1–245110-5.
- [20] Pishnyak OP, Lavrentovich OD. Electrically controlled negative refraction in a nematic liquid crystal. *Appl Phys Lett*. 2006;89:251103-1–251103-3.
- [21] Zhao Q, Kang L, Li B, Zhou J, Tang H, Zhang B. Tunable negative refraction in nematic liquid crystals. *Appl Phys Lett*. 2006;89:221918-1–221918-3.
- [22] Kang L, Zhao Q, Li B, Zhou J, Zhu H. Experimental verification of a tunable optical negative refraction in nematic liquid crystals. *Appl Phys Lett*. 2007;90:181931-1–181931-3.
- [23] Li MS, Huang SY, Wu ST, Lin HC, Fun AYG. Optical and electro-optical properties of photonic crystals based on polymer-dispersed liquid crystals. *Appl Phys B*. 2010;101:245–252.
- [24] Sun J, Zhou J, Li B, Kang F. Indefinite permittivity and negative refraction in natural material: graphite. *Appl Phys Lett*. 2011;98:101901-1–101901-3.
- [25] Chen CY, Tsai TR, Pan CL, Pan RP. Room temperature terahertz phase shifter based on magnetically controlled birefringence in liquid crystals. *Appl Phys Lett*. 2003;83:4497–4499.
- [26] Fan YH, Ren H, Wu ST. Normal-mode anisotropic liquid-crystal gels. *Appl Phys Lett*. 2003;82:2945–2947.
- [27] Maune B, Loncar M, Witzens J, Hochberg M, Baehr-Jones T, Psaltis D, Schere A, Qiu Y. Liquid-crystal electric tuning of a photonic crystal laser. *Appl Phys Lett*. 2004;85:360–362.
- [28] Zhang F, Zhang W, Zhao Q, Sun J, Qiu K, Zhou J, Lippens D. Electrically controllable fishnet metamaterial based on nematic liquid crystal. *Opt Exp*. 2011;19:1563–1568.
- [29] Gorkunov MV, Osipov MA. Tunability of wire-grid metamaterial immersed into nematic liquid crystal. *J Appl Phys*. 2008;103:036101-1–036101-3.
- [30] Khoo IC, Werner DH, Liang X, Diaz A, Weiner B. Nanosphere dispersed liquid crystals for tunable negative–zero–positive index of refraction in the optical and terahertz regimes. *Opt Lett*. 2006;31:2592–2594.
- [31] Wang X, Kwon DH, Werner DH, Khoo IC, Kildishev AV, Shalaev VM. Tunable optical negative-index metamaterials employing anisotropic liquid crystals. *Appl Phys Lett*. 2007;91:143122-1–143122-3.
- [32] Spinozzi E, Ciattoni A. Ultrathin optical switch based on a liquid crystal/silver nanoparticles mixture as a tunable indefinite medium. *Opt Mat Exp*. 2011;1:732–741.
- [33] Gauza S, Li J, Wu ST, Spadlo A, Dabrowski R, Tzeng YN, Cheng KL. High birefringence and high resistivity isothiocyanate-based nematic liquid crystal mixtures. *Liq Cryst*. 2005;32:1077–1085.
- [34] Liao YM, Chen HL, Hsu CS, Gauza S, Wu ST. Synthesis and mesomorphic properties of super high birefringence isothiocyanato bistolane liquid crystals. *Liq Cryst*. 2007;34:507–517.
- [35] Gauza S, Wen CH, Wu ST, Janarthanan N, Hsu CS. Super high birefringence isothiocyanato biphenyl-bistolane liquid crystals. *Jpn J Appl Phys*. 2004;43:7634–7638.
- [36] Xianyu H, Wu ST, Lin CL. Dual frequency liquid crystals: a review. *Liq Cryst*. 2009;36:717–726.
- [37] Xianyu H, Liang X, Sun J, Wu ST. High performance dual frequency liquid crystal compounds and mixture for operation at elevated temperature. *Liq Cryst*. 2010;37:1493–1499.